Controlled Radiation Damage and Edge Structures in Boron Nitride Membranes

Judy S. Kim,* Konstantin B. Borisenko, Valeria Nicolosi, and Angus I. Kirkland*

Department of Materials, University of Oxford, Parks Road, Oxford OX13PH, U.K.

ABSTRACT We show that hexagonal boron nitride membranes synthesized by chemical exfoliation are more resistant to electron beam irradiation at 80 kV than is graphene, consistent with quantum chemical calculations describing the radiation damage processes. Monolayer hexagonal boron nitride does not form vacancy defects or amorphize during extended electron beam irradiation. Zigzag edge structures are predominant in thin membranes for both a freestanding boron nitride monolayer and for a supported multilayer step edge. We have also determined that the elemental termination species in the zigzag edges is predominantly N.

KEYWORDS: radiation damage · boron nitride · edge structure · energetics · transmission electron microscopy

The size, morphology, and surface structures of nanomaterials determine their intrinsic properties and performance. Early research in this field concentrated on zero-dimensional (0D) and one-dimensional (1D) nanostructures, most notably fullerenes (C_{60})[1] and carbon nanotubes,[2] while two-dimensional (2D) nanomaterials were less widely studied. In part, this may have been due to the thermodynamic prediction[3] that atomically thin 2D crystals are not stable in an ambient environment. However, following the discovery of graphene in 2004,[4] there has been considerable research activity in the characterization and potential applications of this and other 2D materials.

Currently, there is significant interest in hexagonal boron nitride (h-BN) due to its structural similarity to graphene. Thin h-BN membranes are fundamentally different from graphene, having a large band gap of 3−6 eV,[5−7] higher chemical and thermal stability,[8−10] and exceptional hardness,[11] making thin sheets of this material potential candidates for use as high-temperature lubricants,[8,10] insulators in memory diodes,[8] or fibers in high-temperature composites.[12] However, 2D h-BN sheets have been relatively recently synthesized, and little is known about vacancy stability and edge configurations in this material, both of which will have a significant effect on the resultant electronic properties and which will play a key role in chemical functionalization.

High-resolution transmission electron microscopy (HRTEM) enables the direct determination of local structure and defect distributions at atomic resolution. There have been HRTEM studies of h-BN monolayers at 300 keV,[13] 200 kV,[14] 120 kV,[14,15] and 80 kV,[14,16,17] and in addition, scanning transmission electron microscope (STEM) imaging at 60 kV[18] of these materials has been reported. However, radiation-induced structural damage potentially limits the use of HRTEM (and STEM) in studies of these materials even at low accelerating voltages. Therefore, in order to clarify the extent to which HRTEM can be used as a reliable structural probe for h-BN and related 2D materials, it is crucial to understand the mechanisms of radiation damage.

In this paper, we report the first systematic study of the structural changes in h-BN membranes prepared by chemical exfoliation, as a function of electron beam dose, particularly with respect to edge geometries and terminations. The advantage of liquid-phase chemical exfoliation is that it enables the fabrication of a large number of thin, large area membranes using common organic solvents. This work is therefore differentiated from previous studies where knock-on damage effects were used to generate locally modified regions of h-BN monolayers by electron- or ion-beam-induced sputtering of micromechanically cleaved multilayer flakes.[14−17] We also highlight the stability of h-BN membranes under HRTEM imaging conditions at electron doses required for high-resolution analysis. Our experimental observations are confirmed by quantum chemical calculations of radiation damage threshold energies for both fully coordinated atoms and

* Address correspondence to judy.kim@materials.ox.ac.uk, angus.kirkland@materials.ox.ac.uk.

Received for review February 10, 2011 and accepted April 21, 2011.

Published online April 21, 2011
10.1021/nn2005443

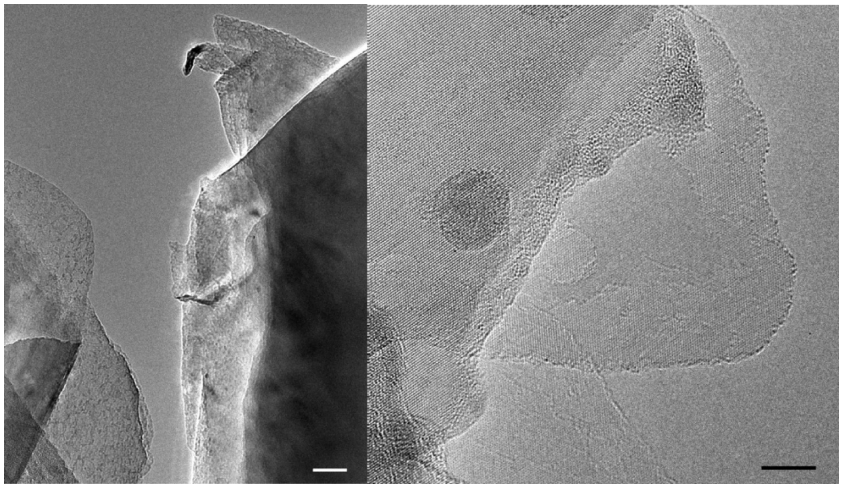

Figure 1. Representative low-magnification TEM images of chemically exfoliated h-BN flakes showing (400−1000 nm^2) thin regions, a few atomic layers thick. At increased magnifications, these are found to contain monolayer subregions. Both micrographs display a 5 nm scale bar.

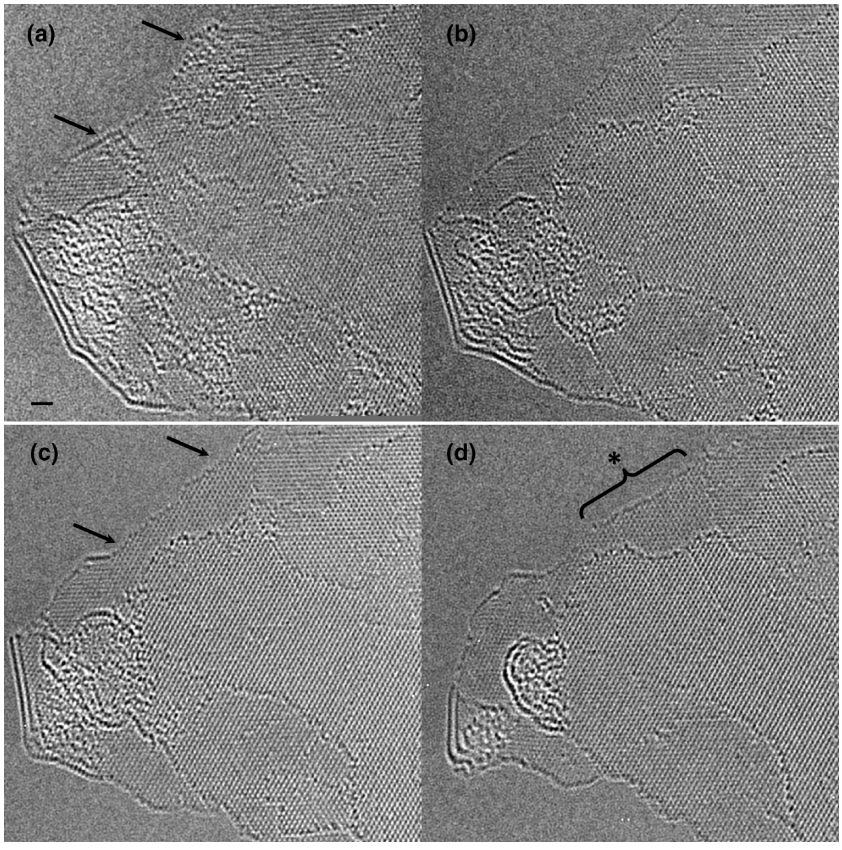

Figure 2. HRTEM images of an h-BN flake recorded after electron doses of (a) 4.6×10^6, (b) 8.0×10^6, (c) 9.5×10^6, (d) 1.5×10^7 e$^-$/Å^2. Reordering of the amorphous material (highlighted by arrows) after exposure to ~9.5×10^6 e$^-$/Å^2 (c) marks a threshold after which the h-BN is clean and subsequently stable for TEM analysis. The region marked with an asterisk * in (d) shows a defect-free monolayer region. Images were recorded at 80 kV at a defocus of 37 ± 1.4 nm, and the scale bar is 1 nm for (a−d).

under-coordinated edge atoms and an examination of the formation energetics of different edge terminations in h-BN.

Thin h-BN flakes were produced by liquid-phase chemical exfoliation of bulk h-BN in *N*-methyl-2-pyrrolidone. This method yields exfoliated flakes with consistently large areas (400−1000 nm^2) of thin, freestanding h-BN (Figure 1) without ionic intercalation or chemical modification through the use of a solvent with a surface energy similar to that of the bulk material.[18−20] These thin regions, as prepared, are typically less than five atomic layers thick and include significant monolayer regions. In comparison, the alternative "Scotch tape" micromechanical exfoliation technique[4,21] is inferior for

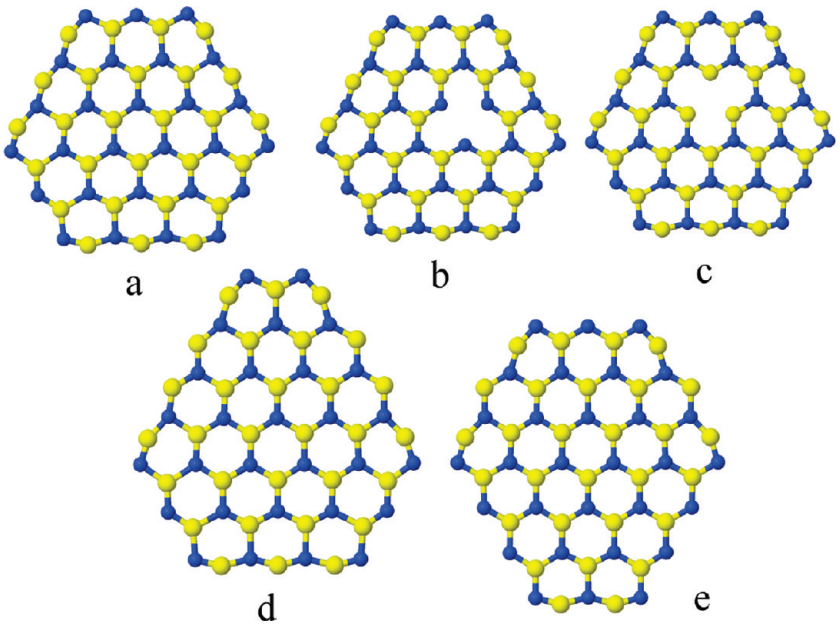

Figure 3. Optimized models of an h-BN flake (a) geometrically ideal structure, (b) B atom vacancy, (c) N atom vacancy. Extended models with additional atoms attached to (d) the N-terminated edge and (e) the B-terminated edge. In all figures, N atoms are shown in blue and B atoms in yellow.

large-scale production of material, which is essential for many potential engineering applications.

RESULTS AND DISCUSSION

Continuous observation of h-BN flakes in an aberration-corrected TEM revealed the effects of electron beam irradiation on the surface and edge structures in the sample. Figure 2 (and Supporting Information video s1) shows changes in a thin h-BN flake as the total electron dose is integrated over many images. At the start of the observation period following exposure to 4.6×10^6 $e^-/Å^2$ (Figure 2a), the h-BN flake is partially covered by amorphous material that is attributed to remnant hydrocarbon adsorbates from the chemical exfoliation process. As the total integrated dose was increased to 9.5×10^6 $e^-/Å^2$ (Figure 2c), the amorphous material undergoes obvious changes, either dissipating into the vacuum or gathering into a localized mass with a smaller surface area and revealing the hexagonal structure of the underlying h-BN membrane. We emphasize that this simple preparation of large, clean regions of uniform membrane thickness makes this material ideal for use as thin freestanding substrates for HRTEM characterization of organic or light element molecules.[22]

In Figure 2a–d, the left side of the flake shows a strong "double-line" feature resulting from curling of the flake edge into a "nanoscroll", similar to the features stabilized by van der Waals forces that have been observed on clean, straight graphene edges.[23] During electron beam irradiation, the scroll shortened as it unrolled and the edge atoms restructured while maintaining the integrity of the neighboring hexagonal membrane structure.

During acquisition of a 20 image focal series (Supporting Information video s2), the monolayer region (shown in the top left region of the flake in Figure 2) shows no vacancies or point defects. This highlights the advantage of using h-BN as a TEM substrate compared to monolayer graphene, which has been studied extensively and has been shown to generate topological defects under 80 kV electron irradiation,[24–26] eventually leading to complete amorphization. This lack of vacancies in monolayer h-BN suggests that it is a naturally more stable supporting structure which is robust to electron beam irradiation. Although our subsequent calculations suggest that this stability is due to differences in the displacement threshold energy for B and N compared to C, the lower chemical reactivity of h-BN sheets compared to graphene may also contribute to a lower rate of beam-induced etching, mediated by free radicals formed from residual contaminants in the microscope vacuum. It is also apparent that the internal monolayer structure of this material is sufficiently stable under electron irradiation conditions for in-depth analysis of exit wave functions restored from focal series image data which improve the overall signal-to-noise ratio and recover the complex exit wave function rather than a real image intensity.[27,28]

In order to understand the enhanced radiation stability observed in h-BN compared to that in graphene, we have calculated threshold energies for atom displacement in these materials. A model of an h-BN sheet consisting of 54 atoms (Figure 3a) was optimized using the Hartree–Fock method with the double-ξ 6-31G basis set[29,30] including a polarization function

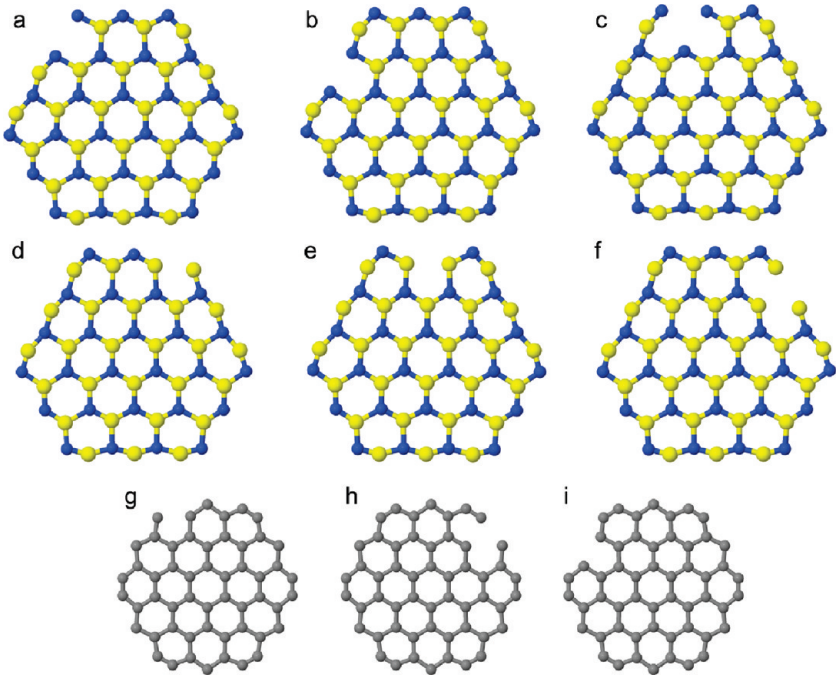

Figure 4. Models of h-BN and graphene flakes with an atom removed from the edge. (a,b) B atom removed from a B-terminated edge. (c) B atom removed from a N-terminated edge. (d,e) N atom removed from a N-terminated edge. (f) N atom removed from a B-terminated edge. (g−i) Carbon atom removed from various positions at the edge of a graphene flake .

implemented in the Gaussian 03 software.[31] Vibrational frequency analysis at the same level was performed to confirm that the optimized structure is the stable state, defined by the absence of imaginary frequencies. To estimate the energy for the displacement of an atom in a homolytic knock-on damage process, single-point energies of structures from which a central atom (either B or N) was removed from the plane of neighboring atoms (Figure 3b,c) and corresponding neutral B and N atoms were computed. In addition, to assess the effect of electron irradiation on the edge of an h-BN flake, an atom from an edge site (Figure 4) was also removed. The damage threshold energy was estimated as a sum of energies for a model with a vacancy, the corresponding displaced atom, and the negative energy of the original undamaged structure. These calculations were performed at the same level of theory. To assess the influence of electron correlation on the computed threshold energy, single-point energy calculations at the MP2/6-31G* level[32] were performed for an initial structure optimized at the HF/6-31G* level and for a structure with either a B or an N atom removed. The energy released during relaxation of the structures following removal of an atom from the flake was calculated by energy optimization of structures with defects at the HF/6-31G* level and subtracting the energy of the original distorted structure. For comparison, similar calculations were also performed for a graphene sheet, from which a carbon atom was removed.

The cross section for isotropic knock-on radiation damage by primary electrons was calculated following Seitz and Koehler[33] as

$$\sigma_d = \frac{Z^2 e^4 (1-\beta^2)}{16\pi\varepsilon_0^2 m_0^2 c^4 \beta^4}\left\{\frac{T_m}{E_d} - 1 - \beta^2 \ln\left(\frac{T_m}{E_d}\right) + \pi Z\alpha\beta\left[2\left(\frac{T_m}{E_d}\right)^{1/2} - \ln\left(\frac{T_m}{E_d}\right) - 2\right]\right\}$$

where Z is atomic number, e is the electron charge, m_0 is the mass of an electron, ε_0 is the dielectric permittivity of free space, c is the speed of light, $\beta = v/c$ with v the speed of electrons in the electron beam, α is the fine structure constant, E_d is the displacement threshold energy, and T_m is maximum transmitted energy in a scattering event given by

$$T_m = \frac{2ME(E + 2mc^2)}{(M+m_0)^2 c^2 + 2ME}$$

where M is the atomic mass of the displaced atom and E is the energy of the electron beam. The results of these calculations are given in Table 1.

Although the static approach used in our calculations estimates only the lower bound of the damage threshold energies, it uses considerably less computational resources than those required for a more complex molecular dynamics simulation. In addition, molecular dynamics simulations may overestimate the radiation damage threshold energies as has been previously reported for graphene.[34,35] Therefore, we believe that static estimates, when made at the same level of theory for two structurally comparable systems (monolayers of h-BN and graphene), are adequate for assessment of the relative radiation stability of these

TABLE 1. Maximum Transmitted Energies, T_m (eV), for Knock-on Radiation Damage by an Electron Beam at 80 keV Together with Displacement Threshold Energies, E_d (eV), Radiation Damage Cross Sections σ_d (barn) at 80 keV, the Electron Beam Energies E (keV) at Which Radiation Damage Is Expected ($E_d = T_m$) and Relaxation Energy Values for Vacancy Formation, ΔE_{relax} (eV) for Atoms in h-BN and Graphene Monolayers: Corresponding Structural Models Are Indicated

		HF/6-31G*				HF/6-31G*//MP2/6-31G*		
displaced atom	T_m	E_d	σ_d	E	ΔE_{relax}	E_d	σ_d	E
central B in BN	17.5	17.1[a]	1.3	79	5.0	18.5		84
edge B in BN[a]	17.5	9.3	53.4			11.9	27.5	
edge B in BN[b]	17.5	10.4	40.7			13.0	20.0	
edge B in BN[c]	17.5	12.5	23.2			15.9	5.6	
central N in BN	13.5	13.5	0.1	80	1.5	17.8		103
edge N in BN[d]	13.5	7.6	91.8			12.2	11.8	
edge N in BN[e]	13.5	10.1	38.2			13.3	1.7	
edge N in BN[f]	13.5	9.2	53.8			13.4	0.9	
central C in graphene	15.8	15.9		81	1.2	17.7		89
edge C in graphene[g]	15.8	8.3	78.5			10.8	38.6	
edge C in graphene[h]	15.8	14.5	6.9			16.5		84
edge C in graphene[i]	15.8	10.2	46.2			11.1	35.1	

[a]Figure 4a. [b]Figure 4b. [c]Figure 4c. [d]Figure 4d. [e]Figure 4e. [f]Figure 4f. [g]Figure 4g. [h]Figure 4h. [i]Figure 4i.

materials. Moreover, in these systems, the differences in displacement threshold energies are expected to come mainly from differences in the bond energies for the displaced atoms, which should be adequately described by static calculations.

The radiation damage threshold energy in a graphene flake computed at the MP2/6-31G* level shows good agreement with the radiation threshold energy obtained previously for carbon nanotubes at 17 eV,[36] while the values computed at the HF level are considerably lower. For comparison, equivalent calculations for graphene predict this energy to be 15 or 22 eV, respectively.[34] Imporantly, the values computed at the HF level suggest that, contrary to our observations, h-BN should be less radiation-stable than graphene. We interpret this as evidence that the results obtained from calculations that include electron correlation are more reliable, and these are therefore used subsequently.

Further examination of the results from our calculations suggests that the radiation damage threshold energies calculated for atoms in the middle of an h-BN flake are in agreement with those computed previously, accounting for the likely overestimate of values from molecular dynamics studies. Using the dynamic approach, previous studies[14] reported E_d values for B as 19.4 eV and for N as 23.1 eV in h-BN sheets.

Displacement threshold energies calculated using extensive molecular dynamics simulations for BN nanotubes under the density functional theory tight binding approximation[37] are also lower (15 eV for B and 14 eV for N atoms), which has been suggested to arise from an inadequate description of charge transfer in the tight binding approximation.[14] Our present calculations result in intermediate values and also indicate a higher value of the radiation damage threshold energy for B atom as compared to N atom, as reported previously.[37]

Our calculations of the radiation damage threshold energy indicate that displacement of a N atom from the middle of the flake requires an energy comparable to that required to displace a C atom in graphene from similar location. However, displacement of a B atom requires a higher energy. According to our calculations of the maximum transmitted energy, taking into account the atomic mass, no central atoms are displaced at 80 keV in either graphene or in h-BN. The electron beam energy that is required to displace a central C atom in graphene is only slightly higher than that required to displace a B atom in h-BN (Table 1). However, displacement of a N atom in h-BN requires considerably higher beam energy.

Our present calculations show that coordinated atoms at the edges, in general, have lower radiation damage threshold energies than atoms in the center of the flakes. In addition, the present calculations of atoms at the edges of graphene flakes are more sensitive to radiation damage than those at equivalent sites in h-BN. It also appears that the most radiation-sensitive atoms in either grapheme or h-BN are C or B atoms, respectively, at the corners of a flake at the intersection of two edges.

Overall, these calculations therefore support our experimental observations of higher radiation stability in an h-BN monolayer compared to that in graphene. For atoms in the middle of the flake, statistically half the atoms in h-BN will have a substantially lower damage cross section compared to graphene, and second, edge atoms are more stable in h-BN than in graphene. These findings also agree with the recent observations that BN nanotubes are more stable than carbon nanotubes under Ar and He ion irradiation.[38]

We have also estimated the energy of vacancy formation in both h-BN and graphene from the energies for structural relaxation after an atom was removed (computed at the HF/6-31G* level) and the damage threshold energies (computed at the HF/6-31G*//MP2/6-31G* level). The energies of B vacancy formation in h-BN, N vacancy formation in h-BN, and the energy of C vacancy formation in graphene are 13.5, 16.3, and 16.5 eV, respectively. Hence, although a B atom possesses a higher knock-on damage energy threshold, it is easier to remove by electron beam irradiation than a N atom due to its lower mass. In addition, there is a larger amount of energy released after B atom removal in the consequent relaxation process, resulting in a lower overall energy associated with the vacancy formation process in h-BN compared

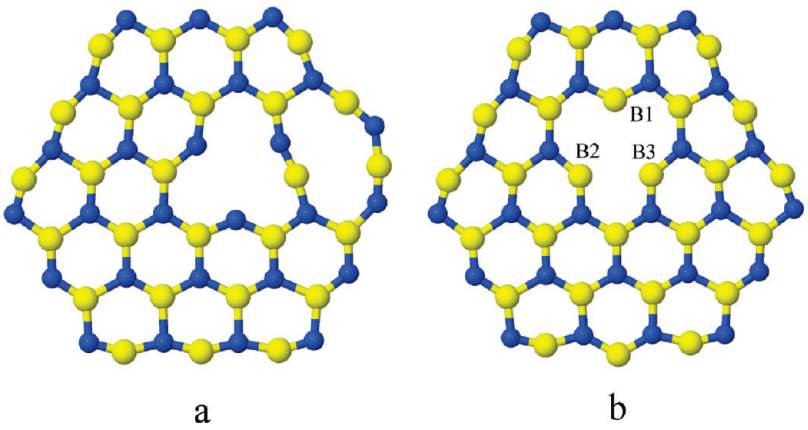

Figure 5. Optimized models of an h-BN flake with (a) B atom vacancy and (b) N atom vacancy.

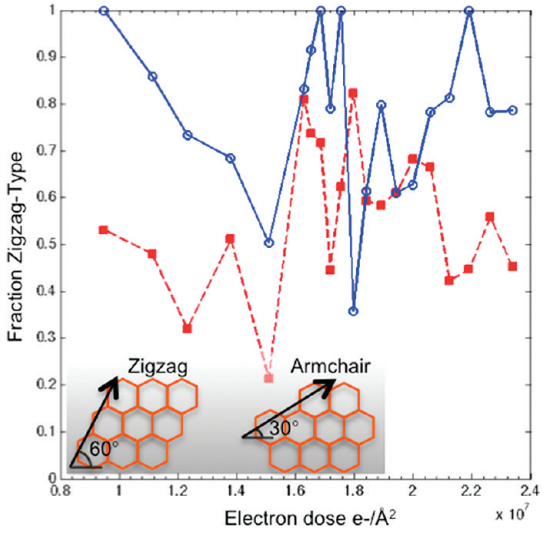

Figure 6. Edge structures in h-BN for a series of images with increasing electron dose from 9.9×10^6 to 2.3×10^7 $e^-/Å^2$. Two types of edges are analyzed: a freestanding monolayer edge (red dashed) bordered by vacuum and a supported multilayer step edge (blue solid) that is supported by another h-BN monolayer membrane. At lower doses, both edge types change toward a greater armchair fraction. At higher dose conditions, there is no systematic trend toward either edge structure. The inset shows a schematic of zigzag and armchair-type edge structures.

to graphene. However, despite this lower energy for vacancy formation in h-BN than in graphene, the kinetic factors represented by the damage threshold energies imply higher radiation stability for h-BN than for graphene. The resultant relaxed structures computed at the HF/6-31G* level are shown in Figure 5.

These calculations indicate that there is a substantial rearrangement of the rings adjacent to the B atom vacancy (Figure 5a). However, this may be due to the close proximity of the vacancy to the edge in the computed model. In the model flake with a N atom vacancy (Figure 5b), there is a considerable differentiation of the B···B distances around the vacancy, with one shorter B2···B3 distance of 0.253 nm and two longer B1···B2, B1···B3 distances of 0.298 nm. For comparison, the B···B distances in h-BN without defects are computed to be 0.247 nm. We also note that both of these structures with single atom vacancies have three unpaired electrons.

It is anticipated that h-BN monolayers containing an even number of total electrons, thus excluding formation of unpaired spin centers, would be the most stable. This condition is satisfied for a structure containing an even total number of atoms and consequently equal numbers of B and N atoms. Only certain configurations consisting of fused rings fulfill this requirement without defects, and importantly, our experimental observations (Figure 2d) suggest that this condition is fulfilled in a monolayer.

For future applications and functionalization of h-BN films, characterization of the edge structures is essential. After significant electron irradiation (1.5×10^7 $e^-/Å^2$) of the h-BN flake, inspection of an experimental focal series of images (Supporting Information video s2) revealed a stable monolayer region with atomic reordering of only the edge atoms. As we have calculated that the monolayer is predicted to lack atomic vacancies (Table 1), edge reconstruction seems the most obvious mechanism for atomic motion. In a similar fashion to graphene,[24] atomic motion at the freestanding edge continuously changes the edge structure from zigzag to armchair arrangements. These results differ from those previously reported for mechanically exfoliated h-BN, where electron or ion beam irradiation generated vacancy holes in the flake interiors[16,15,17] and in which the resultant triangular holes were shown to be terminated with zigzag edges.

In h-BN, zigzag- and armchair-structured edges can be readily identified simply by orienting the image field such that ⟨100⟩ or ⟨2−1−10⟩ directions are aligned to a chosen reference direction. In this configuration, zigzag edges are found at 60° and armchair edges at 30° to the reference direction with a six-fold symmetry. Using this simple method, we have analyzed the proportion of freestanding monolayer and supported multilayer step edges, which are found to be, respectively, 55

and 79% (±15%) zigzag (Figure 6). The remaining interpretable edges are made up of an armchair-type structure, terminated by both B and N atoms. At low electron beam doses (9.9×10^6 to 1.6×10^7 $e^-/Å^2$), an initial decrease in the ratio of zigzag/armchair edge configurations is observed for both freestanding monolayer and supported multilayer step edges, implying that the zigzag edges are destabilized and consequently more armchair edges are formed. With increasing electron dose, the proportion of the two edge configurations varies rapidly with no systematic trend, suggesting that the energy difference between these two configurations is small. Interestingly, preferential formation of zigzag edges was observed in h-BN nanosheets prepared by extended irradiation of BN nanotubes.[39]

As shown in Figure 7, the terminating species in the zigzag edges varies and we have therefore analyzed these from individual images as a function of time. Our assignment of the terminating species is based on analysis of the phase of the reconstructed exit wave (Figure 7a,b). The bright regions in the reconstructed phase represent atomic positions, with N atom sites showing a larger phase shift than B atom sites. Using these assignments of atomic positions, we have determined the edge species in individual images as they change with increasing electron dose. For zigzag edges at the freestanding monolayer flake, the terminating species are 52% (±25%) N, whereas the zigzag edges of the supported multilayer edge are 64% (±17%) N-atom-terminated (Figure 7c). In both cases, the remaining fractions are B-atom-terminated zigzag edges. The terminating species of the zigzag edges at both the supported multilayer and freestanding monolayer are stable at approximately a 50:50 ratio at low electron dose but changes more rapidly at higher dose (1.7×10^7 $e^-/Å^2$) with no obvious systematic trend. Again, this suggests a relatively low energy separation between these two edge configurations.

Returning to simulations for further insight, the energy-optimized structure of the h-BN flake also shows a reconstruction at the edge. The B-atom-terminated edge has an opening of the angle around the B atoms at 151.9° on average, compared to the regular hexagonal angle of 120.0°. The angle around a N atom at the N-atom-terminated edge is 124.6° for atoms in the middle of the edge. However, there is substantial closing (108.1°) of this angle around the N atom that is located at the border between B-atom-terminated and N-atom-terminated edges. The B–N bonds at the edges are also differentiated. In the bulk, the B–N bond is computed to be 0.144 nm, whereas at the N-atom-terminated edge, it is 0.135 nm in the middle of the edge and 0.149 nm at the border with the B-atom-terminated edge. For the B-atom-terminated edge, the equivalent bond lengths are 0.131 nm in the middle of the edge and 0.140 and 0.125 nm at the border with the N-atom-terminated edge.

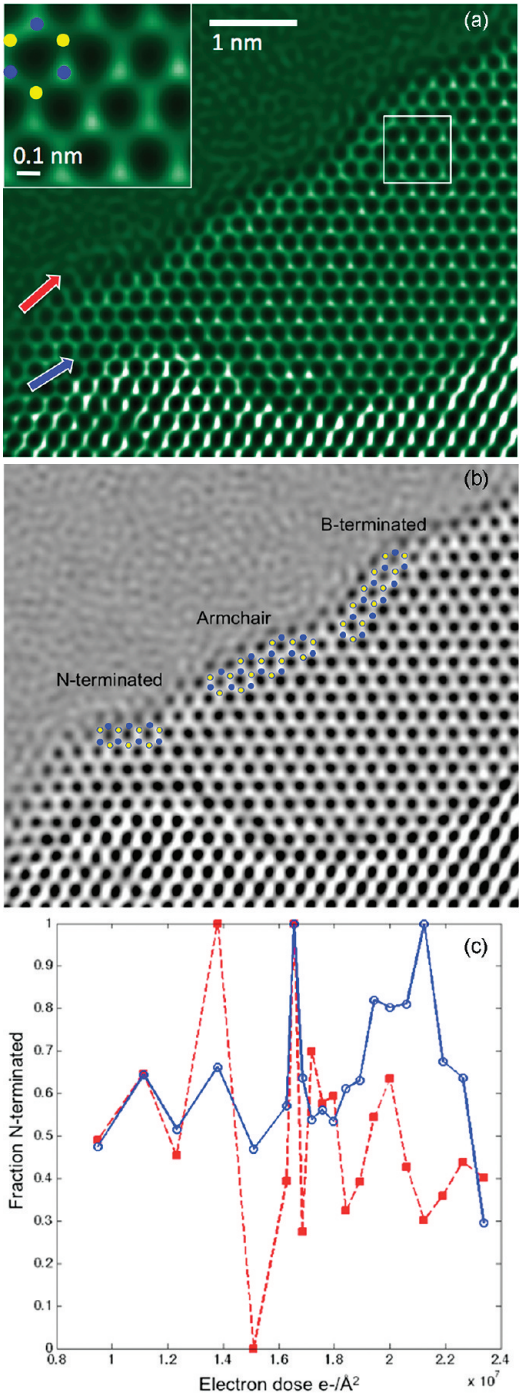

Figure 7. (a) Phase of the reconstructed exit wave of an h-BN monolayer region. Arrows mark the freestanding monolayer edge (red) and the supported multilayer step edge (blue). Images have been oriented to align the ⟨100⟩ direction at 0° with respect to the field of view, making determination of zigzag- or armchair-terminated edges obvious. A higher magnification subregion taken from the area marked by the white box is inset, where N atom positions are shown in blue and B atom positions in yellow. (b) Reconstructed phase including models of the three edge termination types: armchair consisting of both B and N atoms, B-terminated zigzag, and N-terminated zigzag. (c) Elemental edge termination species of zigzag edges with increasing electron dose averaging 52% (±25%) N atom termination for the freestanding monolayer (red dashed) and 64% (±17%) N atom termination for the supported multilayer edge (blue solid).

We have also estimated the relative stabilities of B- and N-atom-terminated edges by computing the energies of geometry-optimized structures at the HF/6-31G* level, where five atoms were added at a N-atom-terminated or B-atom-terminated edge (Figure 3d,e, respectively). The stabilization energies of these extended structures were calculated as the energy difference between the sum of energies of constituent-free atoms and the energy in the extended structure. The additional atoms resulted in excess B atom termination shown in Figure 3d and excess N atom termination shown in Figure 3e. The stabilization energy for the structure with an excess of N-atom-terminated edges was 0.4 eV higher than where there was an excess of B-atom-terminated edges. This suggests that the structure with N-atom-terminated edges is more stable because the energy released during formation of a structure with an excess of N terminal atoms is higher than the energy released during formation of the structure with an excess of B terminal atoms. However, this energy difference at 0.4 eV is relatively small. In addition, the computed energetic preference in edge termination refers to the model structures tested in the present study, and it is possible that different starting model structures show different preferences for edge termination. The experimental observations suggest statistically equal stability for B and N atom edge termination (Figure 7c), but with experimental error hindering a more detailed comparison.

Interestingly, the most stable structure shown in Figure 3e, with an excess of N-terminated edges, was only calculated to be stable with three unpaired electrons, while the structure in Figure 3d was stable with a single unpaired electron, suggesting that N-atom-terminated edges may also affect the magnetic properties of h-BN sheets.

CONCLUSIONS

h-BN represents a largely unexplored 2D material with exotic electronic properties and high specific surface areas with potential in sensing,[40,41] catalysis,[42] and energy storage[43] applications. Facile liquid-phase exfoliation can be employed to produce extended 2D h-BN flakes at low-cost and with high-throughput.[19] Atomic resolution imaging of exfoliated materials is of crucial importance in the characterization of the local structure of monolayers and possible structural defects introduced *via* exfoliation. However, radiation damage is often present at the electron doses used, and for this reason, it is crucially important to assess the radiation stability of this class of material. In multilayer regions of h-BN flakes, defects have been observed at grain boundaries and as single atomic column vacancies, which have minimal mobility within the material.

On the basis of our studies of chemically exfoliated h-BN membranes, we have shown that they are superior to graphene in terms of structural integrity and radiation stability. Quantum chemical calculations for a zigzag-terminated flake suggest considerable rearrangement of the edge structure compared to the bulk, with notable straightening of the B-atom-terminated edge due to opening of the N—B—N angles. The B—N distance also varies with differences of up to 0.024 nm between different bonds.

These calculations and experimental observations also suggest that h-BN is more stable to electron beam irradiation than graphene due to a number of factors. First, the higher mass of N atoms and comparable knock-on damage threshold energies of C and N require higher electron beam energies to displace N atoms from h-BN compared to C from graphene. In addition, the electron beam energy required to displace a B atom from h-BN is comparable to that needed to displace C from graphene. Overall, this statistically produces a more radiation-stable material since, in h-BN, half of the atoms are more radiation-stable than those in graphene. We have also observed that edges in h-BN also appear to be more radiation-stable than the equivalent edges in graphene.

We have also reported the statistics of the edge structure and termination species in h-BN. Our experimental data show a slight preference for zigzag-type edges in h-BN flakes. Large variations in the zigzag edge termination species average *ca.* 50:50 B or N atom, suggesting a similar energetic stability in the two configurations. This is consistent with our calculation of only a relatively small preference for N atom termination in zigzag edges in BN.

METHODS

For HRTEM imaging, a dispersion of thin h-BN flakes was dropped directly onto a standard lacey carbon film TEM grid, allowed to evaporate in atmosphere, then heated in vacuum at 120 °C for 60 min. Prior to insertion into the TEM column, the specimen grid was heated to 80 °C for 15 min in vacuum to remove any remaining solvent that could have readsorbed in order to minimize subsequent reactive etching of the sample by residual organic molecules.

HRTEM images were acquired using a double aberration-corrected JEOL 2200MCO[44,45] instrument operated at 80 kV. Third-order spherical aberration was adjusted to $C_3 = -3\ \mu$m in order to compensate residual fifth-order spherical aberration,[45,46] such that the overall information transfer was limited by chromatic aberration. The remaining residual aberrations to third order were measured and corrected using a Zemlin tableau[47] of power spectra, calculated from images recorded from the amorphous carbon support film, implemented within the CEOS corrector software.[48]

In order to examine radiation damage effects in thin h-BN membranes, the local atomic structure was monitored over a range of electron doses. For the experiments reported here, the

electron dose for a 1 s exposure at 1.5 MX magnification was adjusted to $\sim 2.5 \times 10^4$ $e^-/Å^2$ for a 30 nm illuminating beam diameter at the sample. Microscope-specific calibrations of the beam current were measured using a post-specimen Faraday cup, and the total dose was calculated by considering the total exposure of the specimen during alignment and image acquisition, numbering 167 exposures in total.

Acknowledgment. We thank the Oxford Supercomputing Centre at the University of Oxford for computational support, and S. Haigh for helpful discussions and for providing microscope dose calibrations. Financial Support from EPSRC (Grant reference EP/F028784/1) is gratefully acknowledged.

Supporting Information Available: Short videos of thin h-BN flakes observed using HRTEM illustrating subtle changes in the material with increasing electron dose. Video S1: Changes in an h-BN flake as electron exposure is increased over several minutes. The integrated dose is noted on each frame as electrons/$Å^2$. Video S2: Series of 20 images of an h-BN monolayer region collected with gradually increasing defocus values, used for the exit wave reconstruction. Small changes in the edge structure are evident; however, the interior regions of the flake remain stable. This material is available free of charge *via* the Internet at http://pubs.acs.org.

REFERENCES AND NOTES

1. Kroto, H. W.; Heath, J. R.; O'Brien, S. C.; Curl, R. F.; Smalley, R. E. C60: Buckminsterfullerene. *Nature* **1985**, *318*, 162–163.
2. Iijima, S. Helical Microtubules of Graphitic Carbon. *Nature* **1991**, *354*, 56–58.
3. Mermin, N. D. Crystalline Order in Two Dimensions. *Phys. Rev.* **1968**, *176*, 250.
4. Novoselov, K. S.; Geim, A. K.; Morozov, S. V.; Jiang, D.; Zhang, Y.; Dubonos, S. V.; Grigorieva, I. V.; Firsov, A. A. Electric Field Effect in Atomically Thin Carbon Films. *Science* **2004**, *306*, 666–669.
5. Xu, Y.; Ching, W. Y. Calculation of Ground-State and Optical Properties of Boron Nitrides in the Hexagonal, Cubic, and Wurtzite Structures. *Phys. Rev. B* **1991**, *44*, 7787.
6. Ooi, N.; Rairkar, A.; Lindsley, L.; Adams, J. B. Electronic Structure and Bonding in Hexagonal Boron Nitride. *J. Phys.: Condens. Matter* **2006**, *18*, 97–115.
7. Furthmüller, J.; Hafner, J.; Kresse, G. *Ab Initio* Calculation of the Structural and Electronic Properties of Carbon and Boron Nitride Using Ultrasoft Pseudopotentials. *Phys. Rev. B* **1994**, *50*, 15606.
8. Hirayama, M.; Shohno, K. CVD-BN for Boron Diffusion in Si and Its Application to Si Devices. *J. Electrochem. Soc.* **1975**, *122*, 1671–1676.
9. Schmolla, W.; Hartnagel, H. L. Properties of BN Films Produced by a Low-Temperature Double-Plasma Process. *J. Phys. D: Appl. Phys.* **1982**, *15*, L95.
10. Rand, M. J.; Roberts, J. F. Preparation and Properties of Thin Film Boron Nitride. *J. Electrochem. Soc.* **1968**, *115*, 423–429.
11. Miyoshi, K.; Buckley, D. H.; Pouch, J. J.; Alterovitz, S. A.; Sliney, H. E. Mechanical Strength and Tribological Behavior of Ion-Beam Deposited Boron Nitride Films on Nonmetallic Substrates. *Surf. Coat. Technol.* **1987**, *33*, 221–233.
12. Zhi, C.; Bando, Y.; Tang, C.; Kuwahara, H.; Golberg, D. Large-Scale Fabrication of Boron Nitride Nanosheets and Their Utilization in Polymeric Composites with Improved Thermal and Mechanical Properties. *Adv. Mater.* **2009**, *21*, 2889–2893.
13. Han, W.; Wu, L.; Zhu, Y.; Watanabe, K.; Taniguchi, T. Structure of Chemically Derived Mono- and Few-Atomic Layer Boron Nitride Sheets. *Appl. Phys. Lett.* **2008**, *93*, 223103.
14. Kotakoski, J.; Jin, C. H.; Lehtinen, O.; Suenaga, K.; Krasheninnikov, A. V. Electron Knock-on Damage in Hexagonal Boron Nitride Monolayers. *Phys. Rev. B* **2010** *82*, 113404.
15. Jin, C.; Lin, F.; Suenaga, K.; Iijima, S. Fabrication of a Freestanding Boron Nitride Single Layer and Its Defect Assignments. *Phys. Rev. Lett.* **2009**, 102.
16. Meyer, J. C.; Chuvilin, A.; Algara-Siller, G.; Biskupek, J.; Kaiser, U. Selective Sputtering and Atomic Resolution Imaging of Atomically Thin Boron Nitride Membranes. *Nano Lett.* **2009**, *9*, 2683–2689.
17. Alem, N.; Erni, R.; Kisielowski, C.; Rossell, M.; Gannett, W.; Zettl, A. Atomically Thin Hexagonal Boron Nitride Probed by Ultrahigh Resolution Transmission Electron Microscopy. *Phys. Rev. B* **2009**, 80.
18. Krivanek, O. L.; Chisholm, M. F.; Nicolosi, V.; Pennycook, T. J.; Corbin, G. J.; Dellby, N.; Murfitt, M. F.; Own, C. S.; Szilagyi, Z. S.; Oxley, M. P.*et al.* Atom-by-Atom Structural and Chemical Analysis by Annular Dark-Field Electron Microscopy. *Nature* **2010**, *464*, 571–574.
19. Hernandez, Y.; Nicolosi, V.; Lotya, M.; Blighe, F. M.; Sun, Z.; De, S.; McGovernI., T.; Holland, B.; Byrne, M.; Gun'Ko, Y. K. *et al.* High-Yield Production of Graphene by Liquid-Phase Exfoliation of Graphite. *Nat. Nanotechnol.* **2008**, *3*, 563–568.
20. Coleman, J. N.; Lotya, M.; O'Neill, A.; Bergin, S. D.; King, P. J.; Khan, U.; Young, K.; Gaucher, A.; De, S.; Smith, R. J.*et al.* Two-Dimensional Nanosheets Produced by Liquid Exfoliation of Layered Materials. *Science* **2011**, *331*, 568–571.
21. Meyer, J. C.; Geim, A. K.; Katsnelson, M. I.; Novoselov, K. S.; Booth, T. J.; Roth, S. TheStructure of Suspended Graphene Sheets. *Nature* **2007**, *446*, 60–63.
22. Iijima, S. Thin Graphite Support Films for High Resolution Electron Microscopy. *Micron* **1977**, *8*, 41–46.
23. Gass, M. H.; Bangert, U.; Bleloch, A. L.; Wang, P.; Nair, R. R.; Geim, A. K. Free-Standing Graphene at Atomic Resolution. *Nat. Nanotechnol.* **2008**, *3*, 676–681.
24. Girit, C. O.; Meyer, J. C.; Erni, R.; Rossell, M. D.; Kisielowski, C.; Yang, L.; Park, C.; Crommie, M. F.; Cohen, M. L.; Louie, S. G. *et al.* Graphene at the Edge: Stability and Dynamics. *Science* **2009**, *323*, 1705–1708.
25. Hashimoto, A.; Suenaga, K.; Gloter, A.; Urita, K.; Iijima, S. Direct Evidence for Atomic Defects in Graphene Layers. *Nature* **2004**, *430*, 870–873.
26. Meyer, J. C.; Kisielowski, C.; Erni, R.; Rossell, M. D.; Crommie, M. F.; Zettl, A. Direct Imaging of Lattice Atoms and Topological Defects in Graphene Membranes. *Nano Lett.* **2008**, *8*, 3582–3586.
27. Kirkland, A. I.; Meyer, R. R. "Indirect" High-Resolution Transmission Electron Microscopy: Aberration Measurement and Wavefunction Reconstruction. *Microsc. Microanal.* **2004**, *10*, 401–413.
28. Coene, W.; Janssen, G.; Op de Beeck, M.; Van Dyck, D. Phase Retrieval through Focus Variation for Ultra-resolution in Field Emission Transmission Electron Microscopy. *Phys. Rev. Lett.* **1992**, *69*, 3743.
29. Hehre, W. J. Self-Consistent Molecular Orbital Methods. XII. Further Extensions of Gaussian-Type Basis Sets for Use in Molecular Orbital Studies of Organic Molecules. *J. Chem. Phys.* **1972**, *56*, 2257.
30. Hariharan, P. C.; Pople, J. A. The Influence of Polarization Functions on Molecular Orbital Hydrogenation Energies. *Theor. Chim. Acta* **1973**, *28*, 213–222.
31. Frisch, M. J.; Trucks, G. W.; Schlegel, H. B.; Scuseria, G. E.; Robb, M. A.; Cheeseman, J. R.; Montgomery, J. A., Jr.; Vreven, T.; Kudin, K. N.; Burant, J. C.;*et al. Gaussian 03*, 1st ed.; Gaussian Inc.: Wallingford, CT, 2004.
32. Møller, C.; Plesset, M. S. Note on an Approximation Treatment for Many-Electron Systems. *Phys. Rev.* **1934**, *46*, 618–622.
33. Seitz, F.; Koehler, J. *Solid State Physics*; Academic Press: New York, 1956; Vol. 2.
34. Krasheninnikov, A. V.; Nordlund, K. Ion and Electron Irradiation Induced Effects in Nanostructured Materials. *J. Appl. Phys.* **2010**, *107*, 071301.
35. Krasheninnikov, A. V.; Banhart, F.; Li, J. X.; Foster, A. S.; Nieminen, R. M. Stability of Carbon Nanotubes under Electron Irradiation: Role of Tube Diameter and Chirality. *Phys. Rev. B* **2005**, *72*, 125428.

36. Crespi, V. H.; Chopra, N. G.; Cohen, M. L.; Zettl, A.; Louie, S. G. Anisotropic Electron Beam Damage and the Collapse of Carbon Nanotubes. *Phys. Rev. B* **1996**, *54*, 5927.
37. Zobelli, A.; Gloter, A.; Ewels, C. P.; Seifert, G.; Colliex, C. Electron Knock-on Cross Section of Carbon and Boron Nitride Nanotubes. *Phys. Rev. B* **2007**, *75*, 245402.
38. Lehtinen, O.; Nikitin, T.; Krasheninnikov, A. V.; Sun, L.; Khriachtchev, L.; Banhart, F.; Terao, T.; Golberg, D.; Keinonen, J. Ion Irradiation of Multi-walled Boron Nitride Nanotubes. *Phys. Status Solidi C* **2010**, *4*, 1256.
39. Zeng, H.; Zhi, C.; Zhang, Z.; Wei, X.; Wang, X.; Guo, W.; Bando, Y.; Golberg, D. "White Graphenes": Boron Nitride Nanoribbons *via* Boron Nitride Nanotube Unwrapping. *Nano Lett.* **2010**, *10*, 5049.
40. Ahmad, N.; Lichtman, D. Study of Boron Nitride Thin Films for Ultraviolet Sensor Applications. *Sens. Actuators* **1989**, *18*, 397–405.
41. Huang, Q.; Bando, Y.; Zhao, L.; Zhi, C. Y.; Golberg, D. pH Sensor Based on Boron Nitride Nanotubes. *Nanotechnology* **2009**, *20*, 415501.
42. Centi, G.; Perathoner, S. Catalysis by Layered Materials: A Review. *Microporous Mesoporous Mater.* **2008**, *107*, 3–15.
43. Simon, P.; Gogotsi, Y. Materials for Electrochemical Capacitors. *Nat. Mater.* **2008**, *7*, 845–854.
44. Hutchison, J. L.; Titchmarsh, J. M.; Cockayne, D. J. H.; Doole, R. C.; Hetherington, C. J. D.; Kirkland, A. I.; Sawada, H. A Versatile Double Aberration-Corrected, Energy Filtered HREM/STEM for Naterials Science. *Ultramicroscopy* **2005**, *103*, 7–15.
45. Nellist, P. D.; Kirkland, A. I. Applications of the Oxford-JEOL: Aberration-Corrected Electron Microscope. *Philos. Mag.* **2010**, *90*, 4751.
46. Chang, L.; Kirkland, A.; Titchmarsh, J. On the Importance of Fifth-Order Spherical Aberration for a Fully Corrected Electron Microscope. *Ultramicroscopy* **2006**, *106*, 301–306.
47. Zemlin, F.; Weiss, K.; Schiske, P.; Kunath, W.; Herrmann, K. Coma-Free Alignment of High Resolution Electron Microscopes with the Aid of Optical Diffractograms. *Ultramicroscopy* **1978**, *3*, 49–60.
48. Haider, M.; Uhlemann, S.; Zach, J. Upper Limits for the Residual Aberrations of a High-Resolution Aberration-Corrected STEM. *Ultramicroscopy* **2000**, *81*, 163–175.